⌘ *Author's Choice*

THE JOURNAL OF BIOLOGICAL CHEMISTRY VOL. 284, NO. 10, pp. 6546–6553, March 6, 2009

Crystal Structure of Procaspase-1 Zymogen Domain Reveals Insight into Inflammatory Caspase Autoactivation*[S]

Received for publication, August 7, 2008, and in revised form, December 17, 2008 Published, JBC Papers in Press, December 30, 2008, DOI 10.1074/jbc.M806121200

J. Michael Elliott[‡], Lionel Rouge[§], Christian Wiesmann[§], and Justin M. Scheer[‡1]

From the [‡]Department of Protein Chemistry and [§]Department of Protein Engineering, Genentech, Inc., South San Francisco, California 94080

One key event in inflammatory signaling is the activation of the initiator caspase, procaspase-1. Presented here is the crystal structure of the procaspase-1 zymogen without its caspase recruitment domain solved to 2.05 Å. Although the isolated domain is monomeric in solution, the protein appeared dimeric in crystals. The loop arrangements in the dimer provide insight into the first autoproteolytic events that occur during activation by oligomerization. Additionally, in contrast to other caspases, we demonstrate that autoproteolysis at the second cleavage site, Asp[316], is necessary for conversion to a stable dimer in solution. Critical elements of secondary structure are revealed in the crystal structure that explain why a dimeric protein is favored after proteolysis at this aspartic acid. Dimer stabilization is concurrent with a 130-fold increase in k_{cat}, the sole contributing kinetic factor to an activated and efficient mediator of inflammation.

Caspases are a family of aspartic acid-specific cysteine proteases that are involved in inflammation and apoptosis. This enzyme family is generally categorized into three groups as follows: inflammatory initiators (caspases-1, -4, and -5), apoptotic initiators (caspases-2, -8, -9, and -10), and apoptotic effectors (caspases-3, -6, and -7). Because of its role as the protease responsible for processing prointerleukin-1β (pro-IL[2]-1β) to an active 17-kDa form, caspase-1 is a major driver of inflammation and innate immunity (1–3). The enzyme also participates in the activation of prointerleukin-18 and prointerleukin-33 (4, 5). Caspase-1 activation and the subsequent release of IL-1β, IL-18, and IL-33 are one of the first lines of defense against invading microbes and viruses. Excessive caspase-1 activity, however, can lead to pathologies associated with several autoimmune and inflammatory diseases such as septic shock, inflammatory bowel disease, familial cold autoinflammatory syndrome, rheumatoid arthritis, osteoarthritis, and gout (6–8). Caspase-1 knock-out mice have strongly supported this assertion, demonstrating an absence of processed IL-1β and IL-18 and subsequent decreases in production of cytokines IL-1α, IL-6, interferon-γ, and tumor necrosis factor-α when challenged with lipopolysaccharide or *Listeria monocytogenes* (6, 9, 10). More recent studies have established the involvement of caspase-1 in neurodegenerative disorders such as trauma and ischemic brain injury, Huntington disease, and amyotrophic lateral sclerosis (7).

Pathways leading to the activation of the enzyme are triggered by diverse pathogen and damage-associated molecular patterns such as lipopolysaccharide, flagellin, DNA, RNA, uric acid crystals, bacterial toxins, and UVB damage (11). These patterns are often recognized by Toll-like receptors on the cell surface or by nod-like receptors inside the cell. After pattern recognition, intracellular events result in the conversion of the inactive procaspase-1 zymogen to a fully processed, active enzyme.

Procaspase-1 conversion is induced by macromolecular oligomerization of the proenzyme onto a complex called the inflammasome (11, 12). This process is mediated through recruitment domains in procaspase-1 and inflammasome adapter proteins (13, 14). Upon complex formation, locally high concentrations of the enzyme result in autoproteolysis at three aspartic acids releasing a fully processed, active enzyme. Natural inhibitors of caspase-1 activation include proteins like ICEBERG, Pseudo-ICE/COP, CARD-8, and INCA, which all act as decoys to block recruitment of procaspase-1 to the inflammasome complex (15–19). Oligomerization plays an important role in activation of apoptotic initiator caspases as well, including human caspase-8 and caspase-9 and the *Drosophila* initiator-caspase DRONC.

An effort to synthetically control caspase-1 activity for therapeutic purposes has resulted in the discovery of potent peptidomimetics that inhibit the enzyme at the active site (20). Typically, these compounds rely on caspase preference for substrate with an aspartic acid-like moiety in the P1 position, but this requirement has restricted the design of these inhibitors to small molecules with undesirable specificity and pharmacodynamics (7). Recent structural studies on caspase-1 and caspase-7, however, have shown that allosteric elements can also be targeted by small molecules as an alternative to the active site (21–23). We reasoned that the zymogen activation process could likewise provide a new structural target for therapeutic inhibitors.

Only two caspase zymogen structures are known, human procaspase-7 and the *Drosophila* caspase DRONC, an ortholog

* The costs of publication of this article were defrayed in part by the payment of page charges. This article must therefore be hereby marked "*advertisement*" in accordance with 18 U.S.C. Section 1734 solely to indicate this fact.

The atomic coordinates and structure factors (code 3E4C) have been deposited in the Protein Data Bank, Research Collaboratory for Structural Bioinformatics, Rutgers University, New Brunswick, NJ (http://www.rcsb.org/).

[S] The on-line version of this article (available at http://www.jbc.org) contains supplemental Figs. S1 and S2.

⌘ *Author's Choice*—Final version full access.

[1] To whom correspondence should be addressed. E-mail: scheer.justin@gene.com.

[2] The abbreviations used are: IL, interleukin; CARD, caspase recruitment domain; SEC-MALS, size exclusion chromatography coupled to multiangle light scatter; apo, denoting a ligand free structure; DTT, dithiothreitol; CHAPS, 3-[(3-cholamidopropyl)dimethylammonio]-1-propanesulfonic acid; PDB, Protein Data Bank; r.m.s.d., root mean square deviation; AFC, aminofluoro-coumarin.

of human caspase-9 (24–26). These structures and concurrent studies indicate that the mechanisms of activation differ significantly among caspases. Therefore, using a combination of structural and biochemical methods, we sought to elucidate details of procaspase-1 activation and to provide a basis for novel approaches to inhibitor discovery.

EXPERIMENTAL PROCEDURES

Caspase Expression in Escherichia coli—Wild-type human caspase-1 (residues 104–404 with the active-site residue Cys^{285} mutated to Ala) was cloned into pRSET T7 expression vector (Invitrogen) with an N-terminal Unizyme tag (Unizyme Laboratories). The p20 (residues 121–297) and p10 (residues 317–404) subunits were cloned into the pRSET vector without the affinity tags as described previously (21, 27). Active p35 was cloned into an in-house expression vector pST239 (with supplemental rare tRNA codons ArgU, GlyT, and Pro^2) containing an N-terminal Unizyme tag. pRSET vector constructs were expressed in BL21Star(DE3) cells co-transformed with a rare codon plasmid pRARE2 (Novagen), and constructs using the pST239 vector were expressed in 58F3 cells (derived from W3110 with genotype Δ*fhuA*(Δ*tonA*) Δ*lon galE rpoHts*(*htpRts*) Δ*clpP lacIq* Δ*ompT*Δ(*nmpc-fepE*) Δ*slyD*). BL21Star(DE3) cells were grown in Terrific Broth at 37 °C to 1.0 absorbance at $A_{600\ nm}$, induced with 1 mM isopropyl 1-thio-β-D-galactopyranoside, and allowed to grow overnight. 58F3 cells were grown in phosphate-limiting media at 30 °C to 2–3 $A_{600\ nm}$ before overnight induction with 1 mM isopropyl 1-thio-β-D-galactopyranoside (28).

Purification of p35 C285A—Cell pellets were resuspended in 10× volume of 50 mM Tris, pH 8, 300 mM NaCl, and 5 mM β-mercaptoethanol and homogenized with a Polytron cell grinder followed by four passes through a microfluidizer. The lysate was centrifuged at 20,000 × *g* for 20 min at 4 °C. The supernatant was loaded over a 5-ml HisTrap HP column (GE Healthcare) and washed with 50 mM Tris, pH 8, 300 mM NaCl, 5 mM β-mercaptoethanol. Bound protein was eluted with a 0–250 mM imidazole gradient. The p35 C285A was pooled, diluted, and passed over a 5-ml Q HP HiTrap column. The mutant p35 was recovered from the unbound flow-through, which yielded pure protein (18 mg of soluble protein per liter of cell culture). Unizyme was removed according to the manufacturer's protocol, and the protein was dialyzed into 10 mM Tris, pH 7.5, 100 mM NaCl, and 5 mM DTT prior to crystallography.

Purification and Refolding of Active p35—Cell pellets were passed through a Polytron grinder and microfluidizer in 10× volume of 50 mM Tris, pH 8.0, and 1 M sodium malonate. The lysate was centrifuged at 20,000 × *g* for 20 min at 4 °C. The pellet was solubilized in 6 M GdnHCl, 50 mM Tris, pH 8.0, with 5 mM β-mercaptoethanol using sonication. This extract was centrifuged at 20,000 × *g* for 30 min at 4 °C. Supernatant containing p35 was loaded over a 5-ml HisTrap HP column with 10 mM imidazole, washed with 6 M GdnHCl, 50 mM Tris, pH 8.0, and eluted with the addition of 250 mM imidazole. The eluted p35 protein was purified by S75 (GE Healthcare) gel filtration in 6 M GdnHCl, 50 mM Tris, pH 8.0, and 5 mM β-mercaptoethanol to remove p24 fragments and other contaminants. Refolding and purification was done as described below for $(p20p10)_2$. The refolded protein was dialyzed into 20 mM acetate, pH 5.0, 100 mM sodium malonate, and 5% glycerol at 4 °C. Subsequent secondary dialysis was done in 20 mM acetate pH 5.0, 30 mM malonate, and 5% glycerol.

Purification and Refolding of $(p20p10)_2$—p20 and p10 proteins were refolded at a ratio of 1:1 (2 mg each) by mixing in 50 ml of refold buffer (50 mM HEPES, pH 8.0, 100 mM malonate, 1 M NDSB-201 (nondetergent sulfobetaine-201), 10% sucrose, and 20 mM DTT) as described previously (27). Dialysis and purification were done in the presence of 30 mM malonate.

Analysis of p35 C285A Processing and Dimerization—p35 C285A p35 was mixed with $(p20p10)_2$ caspase-1 at a final concentration of 143 to 1 μM, respectively, in 100 mM HEPES, pH 7.5, 10% sucrose, 0.1% CHAPS, and 10 mM DTT at room temperature. Time points (75 μl of reaction with about 400 μg protein) were centrifuged and analyzed by SEC-MALS (Agilent 1100 high pressure liquid chromatography, Wyatt Technologies miniDawn TriStar, and Optilab DSP). 1 μl of each spun aliquot was also analyzed for protein by SDS-PAGE (4–20% Tris-glycine, Invitrogen). Samples were chromatographed at 1 ml/min in 100 mM HEPES, pH 7.5, 10% sucrose, 0.1% CHAPS, and 10 mM DTT over an S200 Superdex 10/300 GL column (GE Healthcare).

Autoproteolysis of Active p35—p35 was concentrated to 0.5 mg/ml using VivaSpin 0.5-ml, 5-kDa PES concentrators (Sartorius Stedim) and buffer-exchanged with 4× volume of 100 mM HEPES, pH 7.5, 10% sucrose, 0.1% CHAPS, and 10 mM DTT at 4 °C. The protein was brought to room temperature at 0.5 mg/ml, and time points were taken for SDS-PAGE and enzymatic assays. Enzymatic assays were performed at room temperature using reaction buffer (100 mM HEPES, pH 7.5, 10% sucrose, 0.1% CHAPS, and 10 mM DTT) and enzyme concentrations of 20 nM. A caspase-1 substrate titration with Ac-WEHD-AFC (MP Biomedicals) was used to determine K_m values. The irreversible inhibitor benzyloxycarbonyl-VAD-fluoromethyl ketone (not *O*-methylated) (AG Scientific) was used for active-site titrations to determine active-site concentrations. A titration of free AFC (Fluka) allowed for calculation of k_{cat} in moles/s.

Crystallization, Data Collection, and Analysis—p35 C285A crystallized at 4 °C in hanging drops, consisting of a 1:1 ratio of protein (14 mg/ml) to mother liquor, suspended over mother liquor (0.2 M magnesium chloride, 20% (w/v) PEG 3350). Crystals appeared after 2 weeks and grew to their final size of 75 × 75 × 25 μm in 3 weeks. For data collection, crystals were transferred to cryo-buffer containing mother liquor with 20% (v/v) glycerol and then flash-frozen at N_2. Diffraction data were collected from a single crystal at the advanced Light Source (Berkeley, CA) Beamline 5.0.1 to 2.05 Å resolution and was processed using HKL2000 (29). The structure was solved using the program PHASER (30) and the coordinates of 1RWX (31); the model was completed with Coot (32) and refined using REFMAC (33). A Ramachandaran plot using PROCHECK (34) shows some residues in disallowed regions, most of which are found in the poorly ordered section between amino acids 288 and 297.

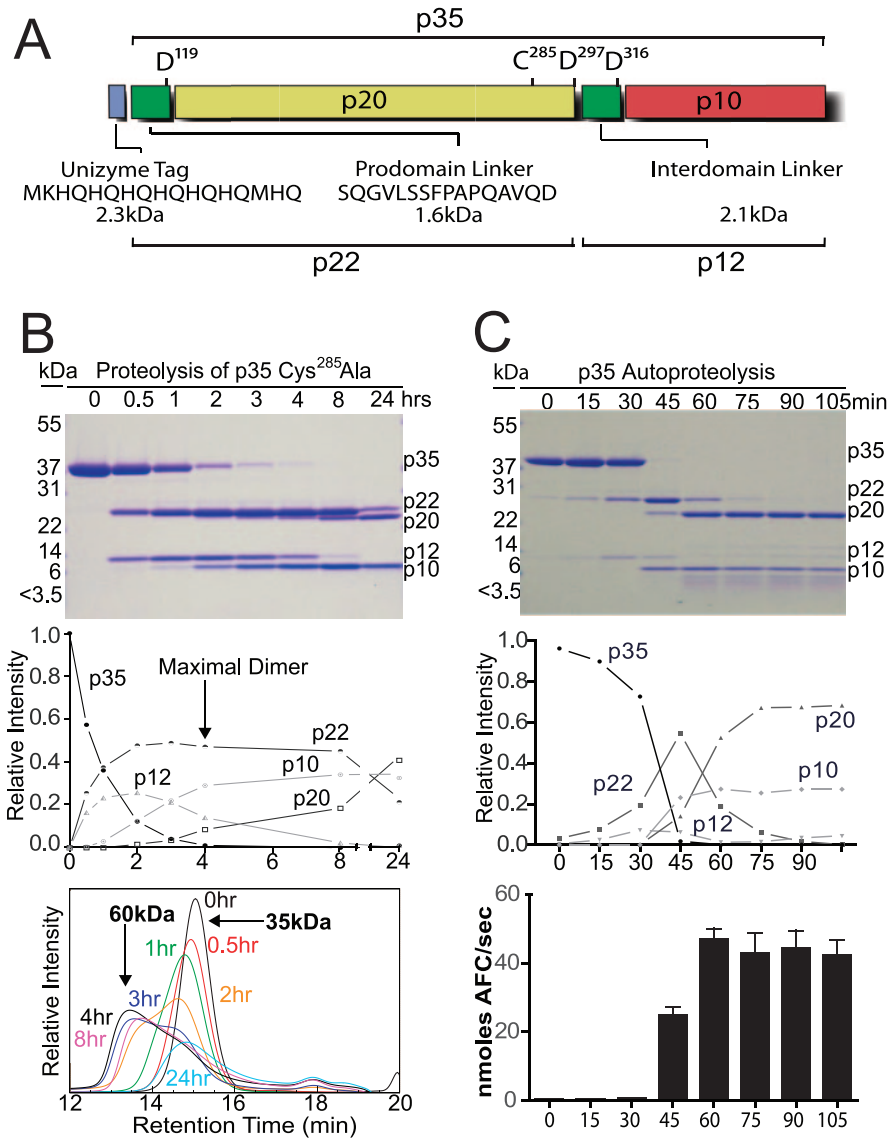

FIGURE 1. **Monomer to dimer conversion of caspase-1 zymogen.** *A,* diagram of p35 expressed in *E. coli* showing common digestion products. *B,* SDS-PAGE separation of time points for p35 C285A digested with a small amount of active enzyme (*upper panel*). The gel was analyzed by densitometry and reported as relative band intensities (*middle panel*). SEC-MALS analysis of 400 μg of protein is shown from each time point (*bottom panel*). *C,* p35 with an intact active-site cysteine was incubated in an enzymatic reaction buffer at 0.5 mg/ml. Time points were taken for 105 min and analyzed by SDS-PAGE (*upper panel*) and densitometry of the gel image (*middle panel*). Enzymatic activity (nanomoles of AFC/s) for each time point was determined with the substrate Ac-WEHD-AFC (*lower panel*).

RESULTS

Caspase-1 Monomer to Dimer Conversion—To understand the biochemical and structural details of the caspase-1 activation process, we characterized the p35 C285A mutant form of the enzyme (Fig. 1*A*). In contrast to purified full-length procaspase-1, which in our hands appeared aggregated (data not shown), the truncated mutant protein could be purified to homogeneity. Analysis by multiple runs of size exclusion chromatography (SEC) coupled with a multiangle laser light scatter (MALS) detection system, a method that allows the measurement of the average molecular mass of eluting peaks, determined that the protein was predominantly monomeric (>98%) even at concentrations greater than 20 mg/ml (~600 μM). To understand what events convert the monomeric protein to a stable dimer of two processed zymogens ($(p20/p10)_2$), we applied a small amount of active caspase-1 to the inactive protein p35 C285A. The proteolytic patterns observed in this experiment (Fig. 1*B*) closely resembled those in cell lysates described previously (35). Our results indicate that the first proteolytic event occurs after Asp^{297} within the large subunit (p20). A second cleavage event then occurs at Asp^{316} resulting in the loss of the linker between the p20 and p10. The third major proteolytic event at Asp^{119} then releases the large subunit from a short fragment connecting the enzyme to the CARD (Fig. 1*B*, *upper* and *middle panels*). All digest time points were analyzed by SEC-MALS, and these data show that after 4 h most of the protein has converted to a species with a molecular mass of 60 kDa, which is expected for the processed dimer (Fig. 1*B*, *lower panel*). Analysis of protein recovery indicates that at all time points about 400 μg of protein was recovered except for at 24 h, where about half that (200 μg) was recovered. Cleavages after 24 h have occurred at position Asp^{381} and Asp^{336} within the p10 subunit accounting for the loss of protein at 24 h and the change in retention time. The actual molar mass of the soluble material based on SEC-MALS analysis is about 45 kDa indicating the loss of a p10 subunit.

Autoproteolysis and Enzyme Activity—We expressed and purified p35 with the active-site cysteine present to determine correlations between proteolysis and enzymatic properties. After changing the buffer to activate the enzyme, the p35 shows complete autoproteolysis over a 90-min time period (Fig. 1*C*). In contrast to the linear rate of digestion observed by treating the inactive protein with a small amount of active enzyme (Fig. 1*B*), the p35 had a dramatic increase in the rate of autoproteolysis once the cleavage process was initiated. As was seen in the digests of the inactive mutant, the order of processing is $Asp^{297} > Asp^{316} > Asp^{119}$. Using the fluorescent substrate Ac-WEHD-AFC, we determined the kinetic constants, k_{cat} and K_m, for the protease at intervals during the processing. The data summarized in Table 1 show that the average K_m value of the enzyme remained constant throughout the experiment at ~4.2 μM, which is equal to the value calculated in other reports (36). Active-site titrations were done for each

TABLE 1
Catalytic properties and cleavage events during the autocatalytic time course of p35 caspase-1

Time point	K_m	k_{cat}	k_{cat}/K_m	Asp^{297}	Asp^{316}	Asp^{119}
min	μM	s^{-1}	$\times 10^5\ M^{-1}\ s^{-1}$	*% cleaved*	*% cleaved*	*% cleaved*
0	3.8	0.054	0.014	3.6	0	0
15	6.2	0.064	0.043	10	0	0
30	5.3	0.103	0.020	27	0	0
45	3.0	3.900	1.30	92	79	20
60	4.0	7.340	1.80	100	96	74
75	3.9	6.720	1.70	100	95	92
90	3.9	6.880	1.80	100	95	97
105	3.3	6.560	2.00	100	95	100

TABLE 2
Diffraction data

	PDB code 3E4C
Space group	P1
Unit cell constants	$a = 56.1$ Å, $b = 58.0$ Å, $c = 119.6$ Å $\alpha = 105.95°$, $\beta = 90.85°$, $\gamma = 92.77°$
Resolution	20 to 2.05 Å (2.12 to 2.05 Å)[a]
R_{sym}[b]	0.058 (0.414)[a]
$\langle I/\sigma I \rangle$	11.2 (1.75)[a]
No. of reflections	114,926
No. of unique reflections	37,223
Completeness	97.0% (87.4%)[a]
Refinement	
Resolution	20 to 2.05 Å
No. of reflections	35,359
R_{work}, R_{free}[c]	0.201, 0.264
No. of non-H atoms	4,423
B-factors	
Overall	36.8 Å^2
Wilson-plot derived	37.5 Å^2
Atoms at 0.5 occupancy	81.2 Å^2
r.m.s.d. bond length	0.012 Å
r.m.s.d. angles	1.4°
Ramachandran plot[d]	86.0, 12.7, 0.8, 0.4%

[a] Numbers in parentheses refer to the highest resolution shell.
[b] $R_{sym} = \Sigma|I - \langle I \rangle|/\Sigma I$, where $\langle I \rangle$ is the average intensity of symmetry related observations of a unique reflection.
[c] $R_{work} = \Sigma||F_o| - |F_c||/\Sigma|F_o|$, where F_o and F_c are the observed and calculated structure factor amplitudes, respectively. R_{free} is the *R*-factor for a randomly selected 10% of the reflections excluded from all refinement.
[d] Percentage of residues in the most favored, additionally allowed, generously allowed, and disallowed regions of a Ramachandran plot (34).

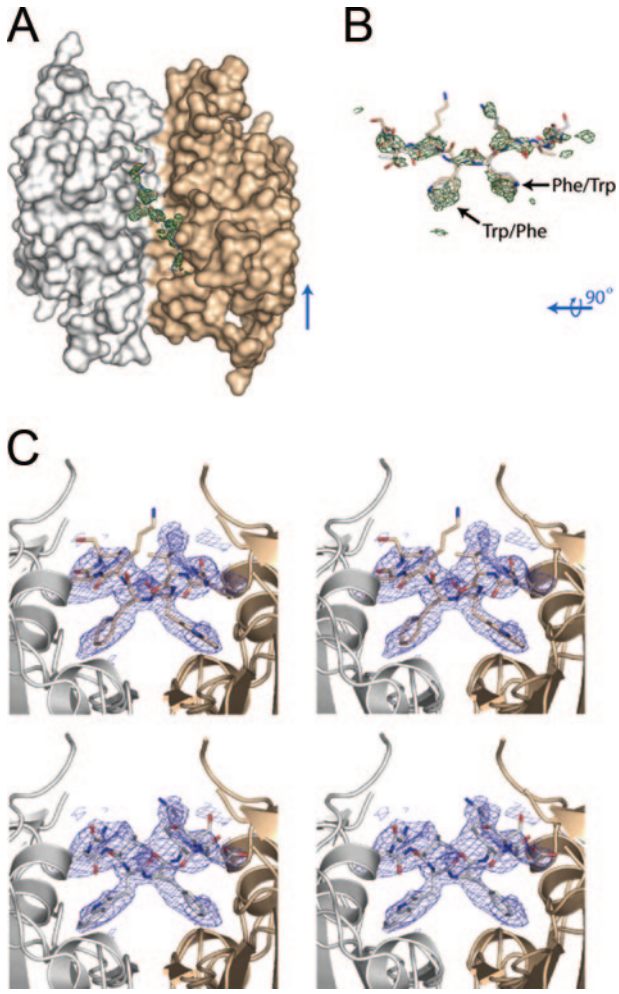

FIGURE 2. **Electron density for residues in the central cavity at the dimer interface.** *A*, surface rendering of the procaspase-1 dimer with electron density $F_o - F_c$ omit map for the area modeled at 50% occupancy. The electron density is contoured at 3σ after refinement and shown in *green*. For better visibility of the cavity, Arg^{240} has been removed from the surface rendering. *B*, residues 291–298 of both chains of caspase-1 within the cavity at the dimer interface are shown along with the $F_o - F_c$ omit map for the area modeled at 50% occupancy. The electron density is shown in *green* contoured at 3σ. *C*, stereo view of the electron density $2F_o - F_c$ contoured at 1σ in the cavity at the dimer interface. The view is oriented lengthwise down the cavity, and the *top panels* show chain A and the *bottom panels* show chain B.

time point, which showed that the number of active sites in the activity assays also remained constant with a concentration of ~7.5 nM. Using a standard curve of free AFC, we calculated the approximate k_{cat} of caspase-1 to be 0.054 s^{-1} at time 0 min and ~7 s^{-1} once fully activated. This represents an ~130-fold increase in k_{cat} upon autocatalytic processing, the only measurable change in caspase-1 kinetic properties. Importantly, analysis of proteolysis patterns on SDS-PAGE indicated that activity was maximal once the interchain linker was completely removed from the small subunit (Fig. 1*C* and Table 1).

Crystal Structure of p35 C285A—The crystals obtained belong to space group P1 and were diffracted to 2.05 Å; the structure was refined to R_{factor}/R_{free} of 20.1/26.4% (Table 2). Although p35 is monomeric in solution, crystals of p35 contained protein dimers. These dimers display the same general architecture observed in all other crystal structures of caspases to date (37). The presence of dimers in the context of protein crystals has been observed in structures for the DRONC zymogen and the processed form of caspase-9, both of which appear predominantly monomeric in solution (24–26, 38–40). An analysis of the surface atoms in the p35 C285A structure using PISA (41) indicates that 11.7% of the total accessible surface area is buried at the dimer interface highlighting the relevance of this interaction.

In the procaspase-1 structure, we initially modeled residues 126–286 and 307–404 for each monomer. In this model, the 20-residue linker (Ser^{104}–Ser^{126}) connecting the CARD domain to the caspase domain is disordered. It is therefore difficult to predict what role the CARD domain may serve structurally within the zymogen. Interestingly, the $F_o - F_c$ electron density map calculated with this model contained additional density when contoured at 3σ in the center of the dimer, near the noncrystallographic 2-fold axis (Fig. 2*A*). This electron density, albeit weak and not well defined, indicates the general position of residues 287–298. Because of the symmetric nature of the caspase dimer, it is possible to fit the side chains of Trp^{294} and Phe^{295} and neighboring residues of either molecule into the most prominent features of the electron density at the center of the dimer (Fig. 2, *A*–*C*). Because of this disorder in the crystals,

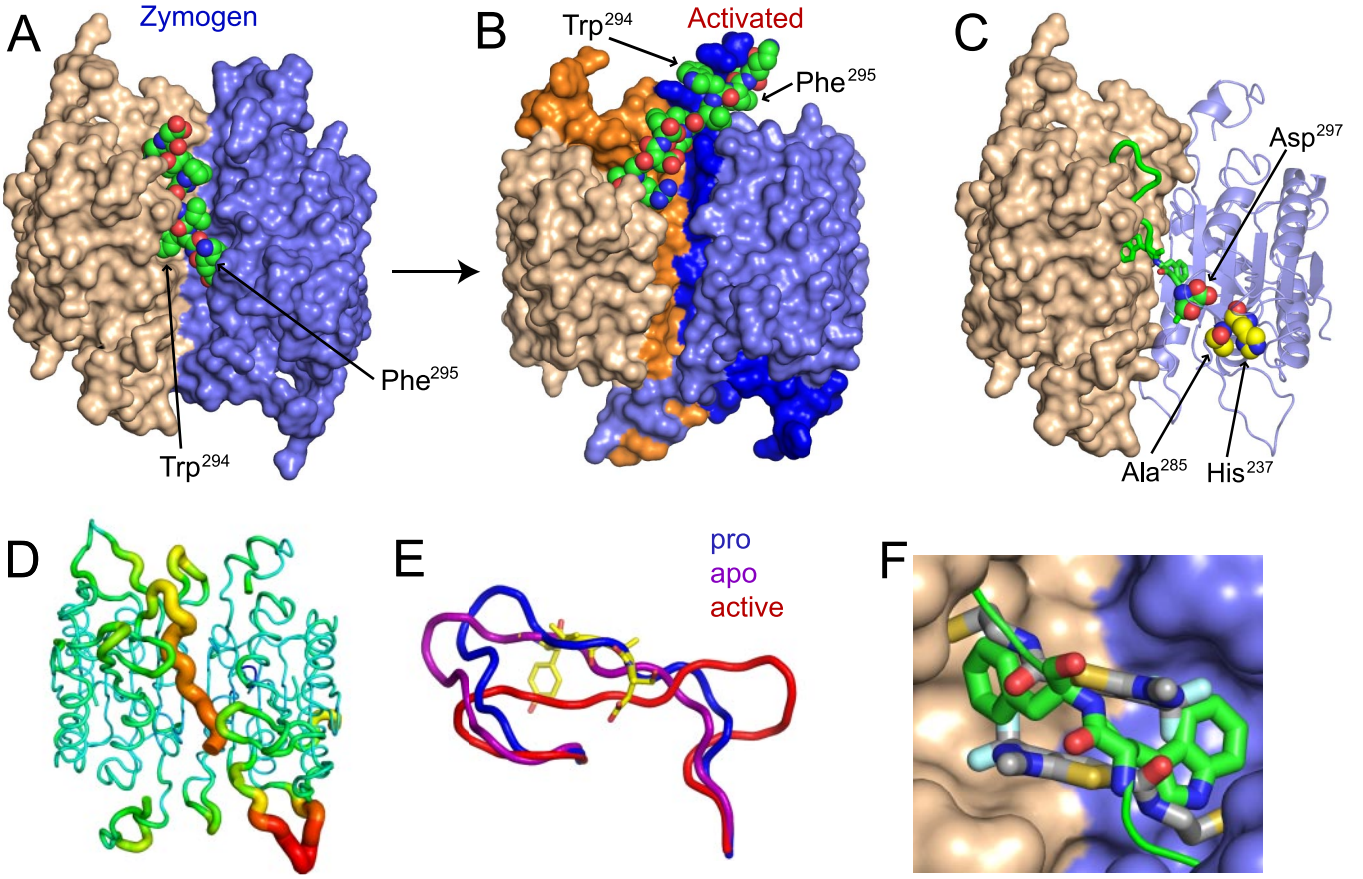

FIGURE 3. **Caspase-1 zymogen in comparison with other caspase-1 structures.** *A,* surface representation of p35 C285A (PDB code 3E4C). The two monomers are colored *wheat* and *slate*, and the residues 286–298 are shown as *spheres* with their carbons colored *green*. Trp^{294} and Phe^{295} are located at the center of the dimeric protein. *B,* surface rendering of the ligand-free, active caspase-1 (PDB code 1SC1 (43)). The p20 and p10 are colored *wheat* and *orange*, respectively, in one subunit, and *slate* and *dark blue* in the other. The central cavity is left unoccupied in this protein because residues 286–298 (shown as *spheres*) are reoriented. *A* and *B*, Arg^{240} has been removed from the surface rendering for visualization of the central cavity. *C,* schematic representation of the subunit on the *right* shows the proximity of Asp^{297} to the adjacent catalytic site (Ala^{285} and His^{237}) in the zymogen structure. *D, B*-factor putty (PyMol) indicates the thermal flexibility of the structure. One active-site loop has less flexibility then the other due to crystal packing. *E,* comparison of active-site loops with or without substrate mimetic. Residues 330–347 are shown as *ribbons* for the apo (ligand-free, *purple*, PDB code 1SC1 (43)), zymogen (*blue*, PDB code 3E4C), and active, inhibitor-bound structures (*red,* PDB code ICE1 (42)). The substrate mimetic in the inhibitor-bound structure, Ac-YVAD-CHO, is colored *yellow*. *F,* hydrophobic pocket binding allosteric inhibitors (*gray sticks*, PDB code 2FQQ (21)) and Trp^{294}–Phe^{295} (*green*).

we modeled residues 287–298 of both molecules with occupancies of 0.5 to indicate that in the crystals the linkers of both molecules occupy the groove in the center of the caspase dimer with about the same probability. Amino acids after Ser^{298}, however, are not defined in the electron density (residues 299–306). SDS-PAGE and N-terminal sequencing analysis of the crystals indicate that the protein was still intact after crystallization (supplemental Fig. S1).

In this final model the two molecules are very similar to each other and superimpose with an r.m.s.d. of 0.61 Å for 269 common C-α atoms. Overall, the dimer of p35 C285A is very similar to the structure of the active enzyme (PDB code 1ICE) (42). The two structures superimpose with an r.m.s.d. of 0.72 Å for 232 C-α positions. However, although the cores of both structures are closely related, there are significant differences at the active-site loops (residues 330–347) that are more like an apo-structure of caspase-1 without an active-site ligand (43). The putative N terminus of the p10 (residues 314–321) subunit, and the linker residues (285–298) are in unique positions in procaspase-1 compared with other structures of caspase-1 and all other caspases (37, 43).

DISCUSSION

The crystal structure of p35 C285A depicts one possible arrangement of the intact polypeptide chains in procaspase-1 dimers at very high concentrations. This arrangement is likely similar to what occurs during oligomerization on inflammasomes and lends support for a mechanism of activation that occurs through intradimer cleavage. This is observed in the C-terminal region of the large subunit, which is positioned along the dimer interface in a cavity that is normally unoccupied in the ligand-free form of the enzyme (Fig. 3, *A* and *B*) (21, 43). The peptide chain undergoes a sharp turn at Gly^{287}, continues for 10 amino acids down the dimer interface, and ends with Asp^{297} positioned very close to the catalytic residue of the neighboring enzyme (Fig. 3*C*). This position is close enough to the catalytic site to allow cleavage of the peptide bond following Asp^{297}. Normally, the aspartic acid side chain of substrate is bound in a positively charged pocket containing Arg^{179} and Arg^{341}, but this pocket is not formed in the zymogen structure because the putative substrate is positioned on the opposite side of the catalytic cysteine. For proteolysis to occur here, only

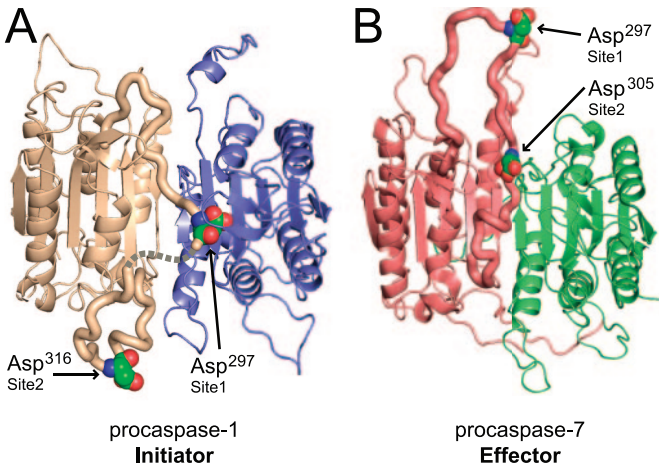

FIGURE 4. **Structural comparison of initiator and effector caspase zymogens.** *A,* procaspase-1 (PDB code 3E4C) shown as a schematic with the linker region shown as a *thick ribbon*. Both aspartic acid cleavage sites between the p20 and p10 in one monomer are shown as *spheres*. The *dotted line* represents unresolved residues not seen in the electron density maps. *B,* schematic representation of procaspase-7 (PDB code 1GQF (25)), an effector caspase, with the interdomain linker shown as a *thick ribbon*. Only the first site of processing in effector caspases is required for activation. It is noticeable that the first cleavage site is up and away from the dimer interface in caspase-7.

the catalytic cysteine needs to reposition for hydrolysis because activity is not absolutely dependent on the other member of the catalytic dyad, His^{237} (42). The carbonyl oxygen of Asp^{297}, however, is within 3.5 Å of the amide nitrogen of Arg^{240} and near the side chains of Arg^{240} and Arg^{286}, which could stabilize a negatively charged transition state and behave like an oxyanion hole. After initial cleavage at Asp^{297} the peptide chain may be less constrained and thus free to exit the cavity at the dimer interface, which would allow space for the adjacent, unprocessed chain to position the second Asp^{297} near the opposite catalytic cysteine. The higher degree of flexibility observed in the active-site and Asp^{297} region (Fig. 3*D*) also suggests flexibility that could accommodate nucleophilic attack of Asp^{297} by Cys^{285} in this region. Alternatively, it could be the exclusion of one linker region from the core of the protein that allows the excluded Asp^{297} to be processed by yet another zymogen neighbor by interdimer cleavage. Arguments have been made for both intradimer and interdimer processing (44, 45), and either scenario would explain how forced dimerization with an inflammasome could activate the caspase-1 auto-proteolytic pathway.

Comparing caspase-1 and caspase-7 zymogens reveals an intriguing difference, the linkers between the large and small subunits start their association with the dimer interface at different points (Fig. 4, *A* and *B*) (24, 25). This altered orientation impacts the location of the first cleavage point in the zymogens. In caspase-1, the first cleavage site of one monomer is buried in the dimer interface near the adjacent catalytic cysteine, whereas in caspase-7 this region is absent from the protein core leaving the first cleavage site exposed. This major difference between an initiator (caspase-1) and an effector caspase (caspase-7) explains the need for oligomerization to start the activation process in caspase-1. Effector enzymes, like caspase-7 and caspase-3, function as downstream components in the proteolytic cascade and do not contain oligomerization or recruitment domains at the N termini. Their zymogens are found dimeric in solution without catalytic activity and are readily activated by cleavage of the interdomain site by upstream initiators (such as caspase-8 and caspase-9). This is in contrast to caspase-1, and other initiator caspase zymogens such as caspase-9 and DRONC, which require some activity as zymogens to autoprocess themselves. Caspase-1, however, apparently differs from these two initiator caspases as cleavage of the enzyme leads to large increases in enzyme activity and dimerization. Caspase-9 and DRONC activation have been shown to be enhanced much more by oligomerization than by proteolysis (39, 40, 46, 47). An interpretation of our combined structural, kinetic, and biochemical data can help explain what is different about caspase-1 and why both dimerization and proteolysis are important for activity.

The low level activity of procaspase-1 has previously been recognized in cell lysates and is characterized kinetically in our report (Table 1) (35). One possibility for the reduced activity of the zymogen could be negative allosteric regulation by the location of the p20 C terminus. An allosteric regulatory site in this region has previously been characterized in both caspase-1 and caspase-7 (21, 23). The tryptophan and phenylalanine that bind in this region occupy a position similar to small molecule-allosteric inhibitors (Fig. 3*F*). However, despite the conserved positioning, the small molecules are more potent because they completely inactivate the enzyme. This may be due to the covalent bond between the small molecules and Cys^{331}. The added effect of this bond could be to completely block protein rearrangement in this region that occurs during substrate binding (see substrate-bound state in Fig. 3*E*). The p20 C terminus, when bound at this site, is likely to be more flexible during active-site binding. This is supported by our kinetic analysis demonstrating that the p35 zymogen likely has the same ability to bind substrate as the fully processed enzyme, observed as a constant K_m (Table 1). Also, the ability of p35 to be completely labeled at the active site by benzyloxycarbonyl-VAD-fluoromethyl ketone confirmed substrate binding (supplemental Fig. S2). These combined data show that k_{cat} is receiving the benefit of interdomain-linker liberation and suggest that despite the unformed substrate-binding site in the crystal structure, caspase-1 can still efficiently bind substrate ligands (Table 1). Thus, the p20 C terminus and linker must affect the k_{cat} by stabilizing the monomer and preventing the cooperative affects of the dimer. What is it then about the interdomain linker in procaspase-1 that imparts monomer over dimer stability?

There is little secondary structure in most of the linker region. After close inspection of the proteolytic events that lead to dimerization, it is clear that the first cleavage at Asp^{297} is not enough to increase k_{cat} or stabilize the dimer. This is certainly different from the executioner caspases, where the initial proteolytic event eliminates the constraint on the linker, which then folds back to form the active-site binding cleft, resulting in a major increase in activity. Conversely, activation occurs after the second cleavage at Asp^{316} in procaspase-1, seen at the 4-h time point in Fig. 1*B* and the 45-min time point in Fig. 1*C* (summarized in Table 1). Because the first cleavage could release the constraint on the linker, it is at first unclear why this is not enough to yield an active enzyme. In the area of the second cleavage, however, is the only well defined secondary struc-

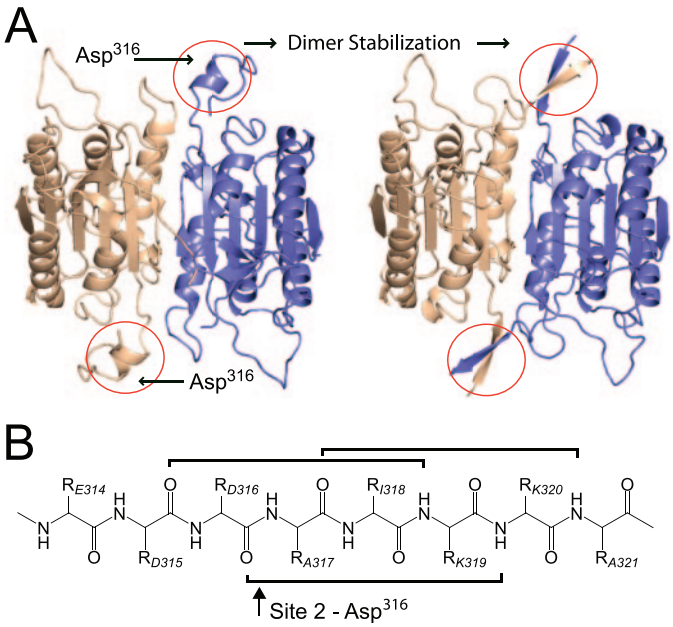

FIGURE 5. **Key structural elements of caspase-1 dimer stabilization.** *A,* schematic representation of caspase-1 zymogen (*left*, PDB code 3E4C) and processed ligand-free caspase-1 (*right*, PDB code 1SC1 (42)). The proenzyme shows a well defined α-helix near the putative N terminus of the p10. This element contains cleavage Site 2, which is the critical processing site for caspase-1 activation. Once proteolysis occurs at Asp^{316}, the newly formed p20 C terminus and p10 N terminus are able to form anti-parallel β-sheets in the active enzyme. The important secondary structural elements are indicated with *red circles*. *B,* diagram of the backbone atoms of residues 314–321. *Brackets* indicate backbone interactions in the α-helix in the proenzyme structure. Two of the three hydrogen bonds in the helix are severed upon proteolysis at Asp^{316}, indicated with an *arrow*.

ture of the linker region, a stable α-helix (Fig. 5*A*). In fact, at this site, Asp^{316} is situated as the penultimate residue of the α-helix. Proteolysis here would eliminate the terminal residues of the helix (Fig. 5*B*). Shortening this stretch of amino acids would destabilize the helix and in turn allow this loop to restructure with the C-terminal region of the adjacent large subunit into an extensive anti-parallel β-sheet. This β-sheet occurs at both poles of the dimeric protein and has been shown to be the most important region for dimer stabilization within caspase-1 (48). Again, this is in contrast to executioner caspases-3 and -7, which have strong β-sheet interaction across the central region of the dimer interface that contribute to the solution state preference for dimerization even before proteolytic activation.

In response to inflammatory signaling, the initial autoactivation of procaspase-1 is triggered by inflammasome oligomerization. The crystal structure provides a view of how autoactivation by intradimer proteolysis at the first cleavage site could result from this forced oligomerization. Proteolysis at the second site, Asp^{316}, converts an α-helix in the monomer to an intradimer β-sheet resulting in a stable dimer with increased enzymatic activity. Thus, the initial instability of the caspase-1 dimer is something that must be overcome during the activation process, *i.e.* a potential target for small molecules that destabilize or prevent the formation of the dimeric form of the enzyme. This type of molecule could eliminate the need for aspartic-acid-containing compounds that treat disorders involving caspase-1.

Acknowledgments—We acknowledge the Advanced Light Source is supported by the Director, Office of Science, Office of Basic Energy Sciences, Materials Sciences Division, United States Department of Energy under Contract DE-AC03-76SF00098 at Lawrence Berkeley National Laboratory. We thank Richard Vandlen for support, guidance, and manuscript review; Jiansheng Wu and Katrina Nicholes for advice and suggestions; and Hok Seon Kim, Dan Yansura, Cecelia Brown, and Art Huang for providing materials.

REFERENCES

1. Black, R. A., Kronheim, S. R., Merriam, J. E., March, C. J., and Hopp, T. P. (1989) *J. Biol. Chem.* **264,** 5323–5326
2. Alnemri, E. S., Livingston, D. J., Nicholson, D. W., Salvesen, G., Thornberry, N. A., Wong, W. W., and Yuan, J. (1996) *Cell* **87,** 171
3. Thornberry, N. A., Bull, H. G., Calaycay, J. R., Chapman, K. T., Howard, A. D., Kostura, M. J., Miller, D. K., Molineaux, S. M., Weidner, J. R., Aunins, J., Casano, F. J., Chin, J., Ding, G. J.-K., Egger, L. A., Gaffney, E. P., *et al.* (1992) *Nature* **356,** 768–774
4. Schmitz, J., Owyang, A., Oldham, E., Song, Y., Murphy, E., McClanahan, T. K., Zurawski, G., Moshrefi, M., Qin, J., Li, X., Gorman, D. M., Bazan, J. F., and Kastelein, R. A. (2005) *Immunity* **23,** 479–490
5. Gu, Y., Kuida, K., Tsutsui, H., Ku, G., Hsiao, K., Fleming, M. A., Hayashi, N., Higashino, K., Okamura, H., Nakanishi, K., Kurimoto, M., Tanimoto, T., Flavell, R. A., Sato, V., Harding, M. W., Livingston, D. J., and Su, M. S. (1997) *Science* **275,** 206–209
6. Joshi, V. D., Kalvakolanu, D. V., Hebel, J. R., Hasday, J. D., and Cross, A. S. (2002) *Infect. Immun.* **70,** 6896–6903
7. Cornelis, S., Kersse, K., Festjens, N., Lamkanfi, M., and Vandenabeele, P. (2007) *Curr. Pharm. Des.* **13,** 367–385
8. Martinon, F., Petrilli, V., Mayor, A., Tardivel, A., and Tschopp, J. (2006) *Nature* **440,** 237–241
9. Kuida, K., Lippke, J. A., Ku, G., Harding, M. W., Livingston, D. J., Su, M. S., and Flavell, R. A. (1995) *Science* **267,** 2000–2003
10. Tsuji, N. M., Tsutsui, H., Seki, E., Kuida, K., Okamura, H., Nakanishi, K., and Flavell, R. A. (2004) *Int. Immunol.* **16,** 335–343
11. Petrilli, V., Dostert, C., Muruve, D. A., and Tschopp, J. (2007) *Curr. Opin. Immunol.* **19,** 615–622
12. Petrilli, V., Papin, S., and Tschopp, J. (2005) *Curr. Biol.* **15,** R581
13. Mariathasan, S., and Monack, D. M. (2007) *Nat. Rev. Immunol.* **7,** 31–40
14. Martinon, F., Burns, K., and Tschopp, J. (2002) *Mol. Cell* **10,** 417–426
15. Druilhe, A., Srinivasula, S. M., Razmara, M., Ahmad, M., and Alnemri, E. S. (2001) *Cell Death Differ.* **8,** 649–657
16. Humke, E. W., Shriver, S. K., Starovasnik, M. A., Fairbrother, W. J., and Dixit, V. M. (2000) *Cell* **103,** 99–111
17. Lamkanfi, M., Denecker, G., Kalai, M., D'Hondt, K., Meeus, A., Declercq, W., Saelens, X., and Vandenabeele, P. (2004) *J. Biol. Chem.* **279,** 51729–51738
18. Lee, S. H., Stehlik, C., and Reed, J. C. (2001) *J. Biol. Chem.* **276,** 34495–34500
19. Razmara, M., Srinivasula, S. M., Wang, L., Poyet, J. L., Geddes, B. J., DiStefano, P. S., Bertin, J., and Alnemri, E. S. (2002) *J. Biol. Chem.* **277,** 13952–13958
20. Scheer, J. M., and Romanowski, M. J. (2009) in *Design of Caspase Inhibitors as Potential Clinical Agents* (O'Brien, T., and Linton, S., eds) pp. 225–250, Taylor & Francis Group, Boca Raton, FL
21. Scheer, J. M., Romanowski, M. J., and Wells, J. A. (2006) *Proc. Natl. Acad. Sci. U. S. A.* **103,** 7595–7600
22. Hardy, J. A., and Wells, J. A. (2004) *Curr. Opin. Struct. Biol.* **14,** 706–715
23. Hardy, J. A., Lam, J., Nguyen, J. T., O'Brien, T., and Wells, J. A. (2004) *Proc. Natl. Acad. Sci. U. S. A.* **101,** 12461–12466
24. Chai, J., Wu, Q., Shiozaki, E., Srinivasula, S. M., Alnemri, E. S., and Shi, Y. (2001) *Cell* **107,** 399–407
25. Riedl, S. J., Fuentes-Prior, P., Renatus, M., Kairies, N., Krapp, S., Huber, R., Salvesen, G. S., and Bode, W. (2001) *Proc. Natl. Acad. Sci. U. S. A.* **98,**

14790–14795
26. Yan, N., Huh, J. R., Schirf, V., Demeler, B., Hay, B. A., and Shi, Y. (2006) *J. Biol. Chem.* **281,** 8667–8674
27. Scheer, J. M., Wells, J. A., and Romanowski, M. J. (2005) *Protein Expression Purif.* **41,** 148–153
28. Simmons, L. C., Reilly, D., Klimowski, L., Raju, T. S., Meng, G., Sims, P., Hong, K., Shields, R. L., Damico, L. A., Rancatore, P., and Yansura, D. G. (2002) *J. Immunol. Methods* **263,** 133–147
29. Otwinowski, Z., and Minor, W. (1997) *Methods Enzymol.* **276,** 307–326
30. McCoy, A. J., Grosse-Kunstleve, R. W., Storoni, L. C., and Read, R. J. (2005) *Acta Crystallogr.* **61,** 458–464
31. Fahr, B. T., O'Brien, T., Pham, P., Waal, N. D., Baskaran, S., Raimundo, B. C., Lam, J. W., Sopko, M. M., Purkey, H. E., and Romanowski, M. J. (2006) *Bioorg. Med. Chem. Lett.* **16,** 559–562
32. Emsley, P., and Cowtan, K. (2004) *Acta Crystallogr.* **60,** 2126–2132
33. Murshudov, G. N., Vagin, A. A., and Dodson, E. J. (1997) *Acta Crystallogr.* **53,** 240–255
34. Laskowski, R. A., MacAurthur, M. W., Moss, D. S., and Thornton, J. M. (1993) *J. Appl. Crystallogr.* **26,** 283–291
35. Yamin, T. T., Ayala, J. M., and Miller, D. K. (1996) *J. Biol. Chem.* **271,** 13273–13282
36. Garcia-Calvo, M., Peterson, E. P., Rasper, D. M., Vaillancourt, J. P., Zamboni, R., Nicholson, D. W., and Thornberry, N. A. (1999) *Cell Death Differ.* **6,** 362–369
37. Fuentes-Prior, P., and Salvesen, G. S. (2004) *Biochem. J.* **384,** 201–232
38. Renatus, M., Stennicke, H. R., Scott, F. L., Liddington, R. C., and Salvesen, G. S. (2001) *Proc. Natl. Acad. Sci. U. S. A.* **98,** 14250–14255
39. Chao, Y., Shiozaki, E. N., Srinivasula, S. M., Rigotti, D. J., Fairman, R., and Shi, Y. (2005) *PLoS Biol.* **3,** e183
40. Snipas, S. J., Drag, M., Stennicke, H. R., and Salvesen, G. S. (2008) *Cell Death Differ.* **15,** 938–945
41. Krissinel, E., and Henrick, K. (2007) *J. Mol. Biol.* **372,** 774–797
42. Wilson, K. P., Black, J. A., Thomson, J. A., Kim, E. E., Griffith, J. P., Navia, M. A., Murcko, M. A., Chambers, S. P., Aldape, R. A., Raybuck, S. A., and Livingston, D. J. (1994) *Nature* **370,** 270–275
43. Romanowski, M. J., Scheer, J. M., O'Brien, T., and McDowell, R. S. (2004) *Structure* (*Lond.*) **12,** 1361–1371
44. Chang, D. W., Xing, Z., Capacio, V. L., Peter, M. E., and Yang, X. (2003) *EMBO J.* **22,** 4132–4142
45. Chen, M., Orozco, A., Spencer, D. M., and Wang, J. (2002) *J. Biol. Chem.* **277,** 50761–50767
46. Bao, Q., and Shi, Y. (2007) *Cell Death Differ.* **14,** 56–65
47. Dorstyn, L., and Kumar, S. (2008) *Cell Death Differ.* **15,** 461–470
48. Piana, S., Sulpizi, M., and Rothlisberger, U. (2003) *Biochemistry* **42,** 8720–8728